Arabian Journal of Geosciences

Origin and Geochemistry of the Late Proterozoic Intra-Arc Rift-Related Volcaniclastic Red And Green Beds of Tayibit El Esm Area, Ablah District, South Central Arabian Shield, Saudi Arabia.

--Manuscript Draft--

Manuscript Number:	AJGS-D-13-00723
Full Title:	Origin and Geochemistry of the Late Proterozoic Intra-Arc Rift-Related Volcaniclastic Red And Green Beds of Tayibit El Esm Area, Ablah District, South Central Arabian Shield, Saudi Arabia.
Article Type:	Original Paper
Abstract:	The volcaniclastic red beds of the study area are present overlying the rhyolite-dolostone succession of wadi Girshah area, Ablah district. It is composed from seven shallowing-upward cycles. The lower part of this sequence is dominated by grey tuffaceous mudstone which grades upward into green tuffaceous mudstone/ siltstone. The middle part is dominated by red hematitic volcaniclastic siltstone- sandstone while the upper part is dominated by thinly to thickly bedded silicified stromatolitic dolostone. This vertical distribution reflects the gradation from deeper conditions of high volcaniclastic input into shallower conditions of very low volcaniclastic input into more shallower and highly restricted depositional environments dominated during the deposition of the uppermost silicicfied dolostones of the upper parts of the succession. The field, mega, microscopic and geochemical results conclude the formation of the present volcaniclastic red beds during the following stages, these are: 1) deposition of the basic and intermediate volcanic ashes in slightly deeper back-arc setting, 2) the degradation of the deposited volcanic ash and the diagenetic authigenesis of green celadonitic clays either along the sediment/water interface or beneath the sea floor by the interaction between Fe2+, Mg2+, Si and Al, 3) the diagenetic hematitization of the formed green celadonitic clays of the cycles of the middle and upper parts of the succession and the formation of the iron-oxyhydroxides mineral .i.e. goethite and hematite as a result of the change in the pore water sediments from reducing to oxidizing conditions, and 4) finally, the direct hematitization of the original tuffaceous materials and formation of iron minerals especially in the upper parts of the volcaniclastic red beds succession.

Origin and Geochemistry of the Late Proterozoic Intra-Arc Rift-Related Volcaniclastic Red And Green Beds of Tayibit El Esm Area, Ablah District, South Central Arabian Shield, Saudi Arabia.

Asaad M. Moufti[1] and Ali A. Mesaed[2]

Faculty of Earth Sciences, King Abdulaziz University

P.O. BOX 80206, Jeddah, 21589, Saudi Arabia

1 ambmoufti@hotmail.com ; 2 Tarefahmed@hotmail.com

Abstract

The volcaniclastic red beds of the study area are present overlying the rhyolite-dolostone succession of wadi Girshah area, Ablah district. It is composed from seven shallowing-upward cycles. The lower part of this sequence is dominated by grey tuffaceous mudstone which grades upward into green tuffaceous mudstone/ siltstone. The middle part is dominated by red hematitic volcaniclastic siltstone- sandstone while the upper part is dominated by thinly to thickly bedded silicified stromatolitic dolostone. This vertical distribution reflects the gradation from deeper conditions of high volcaniclastic input into shallower conditions of very low volcaniclastic input into more shallower and highly restricted depositional environments dominated during the deposition of the uppermost silicicfied dolostones of the upper parts of the succession. The field, mega, microscopic and geochemical results conclude the formation of the present volcaniclastic red beds during the following stages, these are: 1) deposition of the basic and intermediate volcanic ashes in slightly deeper back-arc setting, 2) the degradation of the deposited volcanic ash and the diagenetic authigenesis of green celadonitic clays either along the sediment/water interface or beneath the sea floor by the interaction between Fe2+, Mg2+, Si and Al, 3) the diagenetic hematitization of the formed green celadonitic clays of the cycles of the middle and upper parts of the succession and the formation of the iron-oxyhydroxides mineral .i.e. goethite and hematite as a result of the change in the pore water sediments from reducing to oxidizing conditions, and 4) finally, the direct hematitization of the original tuffaceous materials and formation of iron minerals especially in the upper parts of the volcaniclastic red beds succession.

Keywords: Saudi Arabia, Al Baha, Ablah area, volcaniclastic red beds, rift-related volcanism and sedimentation, green celadonitic clays.

[2] corresponding author: Permanent address: Geology Dept., Faculty of Sciences, Cairo University, El Giza, Egypt.

1. INTRODUCTION

The impact of explosive volcanism on depositional systems has been well documented in recent decades, confirming the generation of eruptive volcaniclastic sequence with a complex stratigraphic architecture (i.e., Vessel and Davies, 1981; Smith, 1987, 1991; Meyer and Dodge, 1988;Waresback and Turbeville, 1990; Riggs and Busby-Spera, 1990; Smith, R.C.M.,1991;Nakayama and Yoshikawa,1997; Bryan et al., 2003). The study of the relations between volcanism and sedimentation are valuable tools in basin analysis. This is because: a) The volcaniclastics represent exotic deposits that are widely dispersed during a very short time interval and they can be used as litho- and chronostratigraphic correlation markers, b) They help in assessing the effect of allocyclic factors, including volcanism and tectonics, on basin sedimentation (Kuenzi et al., 1979; Cas and Busby Spera, 1991; O'Halloran and Gaul, 1997; Riggs et al., 1997; Segschneider et al., 2002; Paredes et al., 2007). The study of Precambrian volcaniclastic successions is very complicated because the pyroclastic deposits are subjected to post-sedimentary modifications involving erosion, alteration, diagenetic compaction or tectonic deformation (Bull and Cas, 1991, 2000; Martí, 1996; Umazano et al., 2008). Combined petrologic and sedimentologic techniques are required to reconstruct the primary features of rocks and the nature of deposits.

In Saudi Arabia, the post amalgamation basins are completely filled with volcaniclastic succession associated with rifting processes post the formation of continent. The term Ablah Formation was first introduced by Brown and Jackson (1960) for the thick volcano-sedimentary in the northern part of the Ablah district in Asir terrane, southwest Saudi Arabia (Fig. 1). Zakir (1972) subdivided the succession of Ablah district into the following rock units: Girshah andesite, Khutnah Formation, Jerub Formation and Ablah Formation. From the economic point of views, Goldsmith (1966), Trent (1966), Trent and Sultan (1966), Theobald and Thompson (1966) and Allcott (1969) have concentrated their works on the economic potential of many mineralized areas within Ablah terrain. Johnson (2006) described the succession of Ablah Formation under the term Ablah group (Cryogenian- Ediacarian layered rocks) and he concluded that, the group is restricted to the volcanic and sedimentary rocks in the vicinity of the Ablah prospect. Recently, the Neoproterozoic volcano-sedimentary succession of Wadi Girshah area has been assigned by Taj. et. al. (2010) to be consists of three main units which represent gradation from inner shelf, shallow marine, lacustrine delta and fluvio-lacustrine environments. They concluded that, this succession was formed during intermittent periods of volcanism; tectonism and sedimentation within inter arc-, back arc-, and intra arc-depositional settings. They subdivided the volcano-sedimentary succession of Ablah area into eleven main volcano-sedimentary rock units disrupted by a series of major strike-slip E-W faults and also by a series of double N-S plunged anticlines. According to Taj et. al. (op.cit), these units are briefly described here as follows:

1) Intermediate volcanic and related volcaniclastics (unit 1) which is represented in the western half of the study area and consists mainly of andesites and related volcaniclastic i.e. volcaniclastic agglomerates and conglomerates.

2) Volcaniclastic green and red beds (unit 2) which consists mainly from the volcaniclastic green and red beds of wadi Halwate.

3) Dolostones and stromatolitic carbonates (unit 3) which almost present above unit 2 in the central part of the study area (Fig. 2). The stromatolitic carbonates of this unit are present in the area west of wadi Girshah (extreme western part of map of Figs. 2, 3).

4) Interbedded dolostone and rhyolite (unit 4) which consists mainly of successive cycles of rhyolite and dolostones and is present in the area between wadi Tayibit El Esm in the east and wadi Girshah in the west.

5) Volcaniclastic conglomerates and sandstones (unit 5): which consists mainly of major successive fining-upward sequences of trough and tabular cross-bedded acidic volcaniclastic conglomerates and agglomerates interbedded with volcaniclastic red beds (the aim of the present study).

6) Acidic volcanics and related volcaniclastic interbedded with dolostones (unit 6): which consists of thinly bedded rhyolite and rhyolitic tuffs intercalated with thinly bedded dolostones.

7) Basic volcaniclastic red beds (unit 7) which consists of a distal volcaniclastic red siltstones and sandstones intercalated with dark green to black tuffaceous siltstones.

8) Basic volcaniclastic agglomerates, conglomerates and volcaniclastic sandstones and siltstones which consists mainly of two main horizons: a lower black volcaniclastic agglomerates interbedded with chloritized and epidoteeitized tuffaceous mudstones and an upper volcaniclastic conglomerates, sandstones and siltstones arranged in fining-upward pattern.

9) Interbedded volcanic and plutonic rocks (unit 9): which are present in the extreme southeastern corner of the study area and consists of interbedded basalts, marbles and fine-grained gabbros with serpentinites.

10) Acidic volcanic and related volcaniclastic unit 10) which consists mainly of interbedded rhyolite and acidic volcaniclastics. This unit is subjected to intensive sheering and metamorphosed to the green schist facies.

11) Quaternary deposits (unit 11): which are represented by wadi fill deposits (10-25m) represent the shallow aquifer of the study area.

The present study aims to give a detailed field, mega- and microscopic description of the volcaniclastic red and green beds of Tayibit El Esm area. The mechanisms of formation and geochemical characters of these green and red beds are also aimed in this study. To achieve these aims, detailed stratigraphic section within the studied volcaniclastic green and red beds was measured (Fig. 2). The collected samples are thin sectioned and the prepared thin sections are described and photo copied. The collected samples are geochemically analyzed by XRF techniques.

2. MATERIALS AND METHODS

The study is based on systematic scientific approach begins with detailed field works including measurement of stratigraphic section of the volcaniclastics unit of Tayibit El Esm area and selecting the most representative hand samples. The selected samples are used in both the thin section preparation and geochemical analyses. The prepared thin sections were carefully described and used in the identification of the petrographic lithotypes as well as the diagenetic processes. The geochemical analyses are used in the interpretation of the field and microscopic data. The results of the field and lab works are summarized in a depositional and diagenetic model of the volcaniclastic green and red beds of the study area.

3. RESULTS OF STUDY

3. 1. Geologic Setting of the Volcaniclastic Red Beds

Tayibit El Esm area is present at the intersection of wadi Raniyah and wadi Girshah (Fig. 2, Fig. 3A). The studied volcaniclastic green and red beds are present within the core of double plunged anticline (Fig. 3B). The stratigraphic section of Tayibit El Esm area (Fig. 4) consists mainly of seven shallowing-upward cycles. These cycles are delineated and terminated by dark green to black basaltic flows (Fig. 3C, D, E, F). The section is dominated in its lower part by grey and green volcaniclastic beds (Fig. 3B, C). Going towards the middle part of the section the shallowing-upward cycles become consists mainly of volcaniclastic red beds. The upper part of the section, the shallowing-upward cycle (cycle 7, Fig. 4) becomes terminated by yellow silicified stromatolitic carbonates (Fig. 3C).

The seven cycles are shown in Fig. 3C. Cycle 1 attain up to 8m thick and it consists of lower grey tuffaceous mudstone (Fig. 4, Column A, Cycle 1). The middle part of this cycle becomes compassed from green tuffaceous mudstone and it terminated by thin black basaltic flow. Cycle 2 attains up to 5m thick and it composed mainly from a basal green tuffaceous mudstone/ siltstone which grades upward into yellow and red volcaniclastic siltstone- fine sandstone and terminated by bench- like red hematitic tuffaceous sandstone (Fig. 4, Upper part of column A). Cycle 3 began by red volcaniclastic sandstone and terminated with basaltic flow. Cycles 4, 5 are nearly similar where they began by green tuffaceous mudstone which grades upward into yellow (cycle 4) or red (cycle 5) volcaniclastic siltstone/ fine sandstone. Both cycles are terminated by basalt flow sheet (middle part of column B, Fig. 4). Cycle 6 is more oxidized where it begins directly by volcaniclastic red siltstone and fine sandstone and terminated by basalt sheet (upper part of column B, Fig. 4). Cycle 7 (attains up to 12m thick, column C, Fig. 4). This cycle begins by very thin (20cm) green tuffaceous mudstone which grades upwards into red mudstone, calcareous mudstone which grades upwards into thinly bedded dolostone. This cycle is terminated with thickly bedded light yellow to white silicified stromatolitic dolostone (marble).

3. 2. Petrographic Description of The Volcaniclastic Green and Red Beds

Detailed petrographic description of the different horizons of the above describe cycles, revealed the recognition of fifteen petrographic lithotypes which are arranged here from base to top (from cycle to cycle 7) and described in the following lines:

3. 2. 1. Grey Tuffaceous Mudstone Pt1

This petrographic lithotype is recorded by a characteristic thick grey unit in the lower part of cycle No. 1 (Fig. 4). It consists of massive grey to black isotropic tuffaceous material contains silt-sized quartz grains (Fig. 5A). Small microcrystalline quartz domains are seen present in association with the silt-sizes quartz grains. These domains are mostly formed by the devitrification of the tuffaceous materials. This grey tuffaceous mudstone also contains small authigenic feldspar crystals and numerous devitrified volcanic domains and patches (Fig. 5B).

3. 2. 2. Hematitic Tuffaceous Siltstone Pt2

This petrographic lithotype is recorded in the middle part of the shallowing-upward cycle just overlying the green celadonitic siltstone and underlying the tuffaceous basalt. It consists mainly of angular to subrounded silt-sized quartz grains embedded in partially to completely hematitized interstitial tuffaceous matrix (Fig. 5C). The quartz grains becomes partially to completely corroded and embayed by the enclosing hematite cement forming dark patches and domains (pseudo-peloids, Fig. 5D). Most of the observed quartz grains seem to be formed by progressive and subsequent stages of digenetic devitrification of small volcanic domains (Fig. 5D).

3. 2. 3. Hematitized Chloritized Tuffaceous Basalt Pt3

This petrographic lithotype is recorded in the black basalt bed terminating the first cycle (Fig. 4). It consists of lath-like interlocked plagioclase crystals embedded in green intensively chloritized volcanic glass and olivine and pyroxene microlites (Fig. 5E). The chloritized olivine and pyroxene crystallites become progressively hematitized into blood red Fe-oxyhydroxides (Fig. 5E).

3. 2. 4. Green Celadonitic Tuffaceous Mudstone / Siltstone Pt4

Which is recorded in the lower and middle parts of the second cycle. It consists of green tuffaceous materials contain silt-sized quartz grains (Fig. 5F). This petrographic lithotype consists mainly of well sorted, angular to subrounded silt-sized quartz grains embedded in grey tuffaceous mudstone matrix (Fig. 5F). This matrix is slightly calcitized in some domains (Fig. 5F).

3. 2. 5. Thinly Laminated Hematitic Tuffaceous Siltstone Pt5

This petrographic lithotype is recorded in the upper part of the 2^{nd} cycle. It consists of rhythmically alternating Fe-rich clayey hematitic laminae alternating with quartz-rich light laminae (Fig. 5G). The dark hematitic laminae show a characteristic mottling appearance where dark brown to black hematitic patches are present within blood red Fe-oxyhydroxides ground mass (Fig. 5H). The quartz grains are intensively corroded and embayed by the enclosing Fe-oxyhydroxides (Fig. 5H). The petrographic lithotype consists mainly from moderately to well sorted quartz grains embedded in slightly to highly hematitized tuffaceous matrix (Fig. 5G, H). Some grey microcrystalline domains were formed by the devitrification of small volcanic domains (Fig. 5H). Some muddy and silty patches are present within this tuffaceous sandstone (Fig. 5G).

3. 2. 6. Calcitized Tuffaceous Mudstone Pt6

Which is recorded in the lowermost part of the 3^{rd} cycle. It consists of green tuffaceous mud suffered from subsequent stages of diagenetic calcitization and formation of micrite or microspar in between the quartz grains (Fig. 6A). It consists mainly dark grey tuffaceous material contains small reddish white calcite aggregates (Fig. 6A). Some microcrystalline quartz aggregates are seen within the tuffaceous materials (Fig. 6A).

3. 2. 7. Laminated Calcareous Siltstone pt7

Which is recorded in the lowermost part of cycle 3. This petrographic lithotype consists of laminated calcitized tuffaceous mudstone and tuffaceous siltstone (Fig. 6B). The contacts between these two laminae is gradational. It consists of silt-sized moderately sorted quartz grains embedded in partially to completely calcitized tuffaceous mudstone (Fig. 6B).

3. 2. 8. Laminated Tuffaceous Hematitic Sandstone Pt8

Which is recorded in the middle part of cycle 3. It consists of rhythmic alternating bands of green celadonitic siltstone parallel to reddish green slightly hematitic celadonitic siltstone (Fig. 6C). The slightly hematitized laminae consists mainly of quartz grains cemented by blood red to black hematite cement. In the highly hematitized laminae, the quartz grains are highly corroded and embayed by the enclosing hematite cement (Fig. 6C). Some blood red to black hematite domains are seen empty from the quartz grains (Fig. 6C).

3. 2. 9. Hematitized Trachytic Doleritic Basalt Pt9

Which is recorded in the topmost part of cycle No. 3. It consists mainly of lath-like sanidine crystals embedded with less frequent Ca-plagioclase crystals (Fig. 6D). Intensively celadonitized, chloritized and calcitized Ca-plagioclase embedded in Fe-rich chloritized and celadonitized olivine and pyroxenes are also observed (Fig. 6D).

3. 2. 10. Thinly Laminated Green Celadonitic Mudstone / Siltstone Pt10

Which is recorded in the middle part of cycle No. 5. It consists of parallel laminated green celadonitic mudstone and celadonitic siltstone (Fig. 6E). The green celadonitic siltstone laminae are usually dense and contain some chlorite flasers and stringers (Fig. 6E).

3. 2. 11. Thinly Laminated Calcitized Mudstone Pt11

Which is recorded in the middle part of cycle 5. It consists mainly of thinly laminated green celadonitized calcitized mudstone parallel to completely calcitized laminae. Sporadically distributed very small silt-sized quartz grains are usually seen within the celadonitized and chloritized laminae. This petrographic lithotype consists of microcrystalline calcite (micrite) (Fig. 6E). Some light color coarse crystalline calcite domains are seen formed by the diagenetic recrystalline of the precursor micrite. In these coarse crystalline calcite domains, quartz crystals are seen (Fig. 6E).

3. 2. 12. Myrmikitic Fine Granite/Rhyolite Pt12

This petrographic lithotype is present in the upper part of cycle 5. It consists of orthoclase, albite with less frequent quartz. It is characterized by the presence of myrmikitic texture (Fig. 6F).

3. 2. 13. Celadonitized and Chloritized Doleritic Basalt Pt13

Which terminate the 5^{th} cycle in this red beds succession. It consists from highly disrupted intensively chloritized, celadonitized and finally oxidized olivine and pyroxene crystallites and ground mass in between calcitized Ca-plagioclase crystals (Fig. 6G). Some hematitized black and blood red (reddish brown) patches and intersected laths patches and domains are usually observed in the chloritized olivine and pyroxene groundmass.

3. 2. 14. Green Calcitized Mudstone Pt14

Which is recorded in the thinly laminated lower part of cycle 7. It consists mainly of partially to completely calcitized tuffaceous mudstone.

3. 2. 15. Chertified and Calcitized Dolostone Pt15

Which is recorded in the middle and upper parts of the shallowing-upward cycle No. 7. It consists of completely calcitized fine- grained dolomite forming microsparry calcite (Fig. 6H). Ultimate stages of diagenetic recrystallization and certification led to the formation of microcrystalline quartz patches and domains within the bedded dolostones of the uppermost part of the succession. The calcite is completely replaced by microcrystalline quartz patches and domains.

3. 3. Geochemistry of the Volcaniclastic Green and Red Beds

Twelve samples are selected from the different horizons of the volcaniclastic-bearing cycles. The samples are carefully selected to be matched with the described petrographic lithotypes. The results of the geochemical analyses are represented in table 1. The colors are used in this table to facilitate the results of the analyses with the lithology of the different horizons. The analyses no. 21pt1 to 23 pt3 are for the samples of the first (lowermost) cycle, and they show the highest Al_2O_3 content because they represent the petrographic lithotypes pt1 , pt2, pt3 which are composed mainly from tuffaceous mudstones and siltstones. The bases of the other cycles are relatively of lower Al_2O_3 content than the base of the first cycle.

The Fe_2O_3 ranges from 3.14 to 10.01%, the high Fe_2O_3 content is present in the basaltic flows terminating the shallowing-upward cycles. Generally, the Fe_2O_3 values are less than 15% which assigned these beds the term “red beds” and not ironstones (Young, 1989). CaO ranges from 0.79 to

10.64%, the high CaO values are present in the middle parts of the cycles within the volcaniclastic red beds. MgO ranges from 0.48 to 9.5. The highest MgO values are present associated with the volcaniclastic red beds. MnO is very low where it ranges from 0.03 to 0.22. Na_2O ranges from 0.69 to 2.35. The highest Na_2O_3 values are present within the basaltic flow beds terminating the volcaniclastic red beds-bearing cycles. K_2O ranges from 0.57 to 2.02. The highest K_2O values are present within the middle and upper parts of the shallowing-upward cycles.

The rare and trace elements distribution show nearly normal values except the Ba and B which are of very high values when compared with the other elements. The high Ba content is matched well the deposition of the volcaniclastic sequence in slightly restricted depositional environments. Ba and B are of high values in the base of the first cycle and after this horizon, B becomes enriched in the different horizons of the cycles.

The variation diagrams of Figure 7 show the positive relation between Fe_2O_3 and TiO_2 (Fig. 7A) also the very low TiO_2 and Fe_2O_3 content except two samples where the Fe_2O_3 reach up to 10 and the TiO_2 reach 2.5. There is also a negative relation between Al_2O_3 and Fe_2O_3 (Fig. 7B). There is a strong positive relation between Fe_2O_3 and Zn (Fig. 7C). Also, there is a negative relation between Cu and Fe_2O_3 (Fig. 7D).

3. 4. Diagenetic Processes

The main diagenetic processes that led to the formation of the volcaniclastic red beds succession of Tayibit El Esm area are deduced by the detection of the precursor constituents that deposited and also the impact of the diagenetic processes on these constituents. These processes include:

3. 4. 1. Devitrification of the Tuffaceous Materials

3. 4. 1. 1. Devitrification of tuffaceous materials

The precursor tuffaceous interstitial material becomes firstly non-crystalline and isotropic (Fig. 8A, B). During the progressive stages of diagenetic recrystallization, it becomes crystalline giving rise to small quartz aggregates (Fig. 8C, D). Ultimate stages of devitrification of the tuffaceous matrix led to the conversion of the microcrystalline quartz aggregates into pseudo-quartz grains.

3. 4. 1. 2. Devitrification of the volcanic grains

In this stage of devitrification, the volcanic grains of the tuffaceous sandstones become initially recrystallized giving rise to microcrystalline quartz aggregates (Fig. 8E, F). Progressive and ultimate stages of devitrification led to the formation of microcrystalline quartz aggregates and patches.

3. 4. 2. Calcitization of the Precursor Tuffaceous Materials

The calcitization of the tuffaceous materials is predominated in the petrographic lithotypes of uppermost parts of the shallowing-upward cycles. This calcitization a process is either occurs on the peripheral parts of the black isotropic material (Fig. 8G) or by entire calcitization and formation of microcrystalline carbonate aggregates (Fig. 8H). This type of entire calcitization is usually associated with the devitrification and formation of microcrystalline quartz (Fig. 8H). In the uppermost parts of the shallowing-upward cycles, the tuffaceous materials show progressive crystallization and formation of microcrystalline calcite patches and domains (Fig. 9A). The microcrystalline calcite patches become progressively recrystallized into coarse crystalline blocky calcite. Ultimate stages of recrystallization led to the formation of blocky calcite showing some signs of silicification and formation of some quartz patches and domains (Fig. 9B). In some domains, the precursor tuffaceous material becomes entirely calcitized giving rise to non crystalline micritic calcite in the interstitial spaces between the isotropic volcanic grains (Fig. 9C, D).

3. 4. 3. Greening (Celadonitization) of the Precursor Tuffaceous Materials

This process is dominated in the green tuffaceous mudstone / siltstone of the middle parts of the 2nd and 3rd cycles of the studied sequence. The microscopic examination of the green tuffaceous mudstone/siltstones of these horizons revealed the presence of green celadonitic clays in the interstitial spaces between volcaniclastic grains (Fig. 9E, F). Also, the volcanic grains of these mudstones and siltstones are also altered to green celadonitic clays (Fig. 9E, F). In some domains, some green celadonitic clay patches and domains become formed within the precursor tuffaceous materials (Fig. 9G, H). The contact between these patches and the enclosing ungreened tuffaceous matrix is gradational. Mesaed (1999a, b) and Mesaed and Surour (2000) postulated the formation of green glauconitic clay by synsedimentary authigenic processes by the reaction between K, Fe^{2+}, Mg, K in slightly reducing conditions. The green glauconitic and celadonitic clays of the lower parts of the shallowing-upward cycles of Tayibit El Esm section are also beer features suggesting during slightly reducing condition, these are: 1) the deep grey color of the tuffaceous mudstone, 2) the absence of red hematitic staffs, 3) the thin lamination characters of the tuffaceous mudstones, 4) the predominance of green colors in the lower parts of the section and red beds in the middle and upper parts of the succession, and 5) the absence of the any sedimentary structures suggesting the predominance of current and wave actions (cross- laminations and cross- bedding).

3. 4. 4. Hematitization Processes and Formation of Red Beds

3. 4. 4. 1. Hematitization of precursor tuffaceous materials

It is observed here that, the main processes that involved in the formation of the red beds of Tayibit El Esm area is the hematitization of different constituents of the volcaniclastic constituents and formation of iron oxyhydroxides minerals (Fig. 10A, B). The hematitization of the interstitial tuffaceous materials is contemporaneous with the processes of devitrification of the volcanic grains and formation of aggregates of microcrystalline quartz (Fig. 10C, D). Two mineral phases of Fe is present i.e. blood red amorphous and the black (Fig. 10C, D). The microscopic observations,, support the processes of diagenetic recrystallization and dehydration of the amorphous blood red phase (geothite) in to the black massive hematite (Fig. 10D, E, F). This is evidenced by the presence of small black hematite patches and domains within the blood red phase (Fig. 10F). Van Houten (1968, 1972) studied the mechanisms of formation of red beds and he proposed the formation of hematite by *in situ* diagenetic conversion of detrital yellow or brown iron oxides derived from deeply weathered, but not necessarily red soils. The hematitization processes is mostly occurred during the late stages of diagenesis. This is evidenced by the patch nature of the hematitic domains and the presence of slightly hematitized domains (Fig. 11A, B, C). The quartz grains show progressive and subsequent stages of corrosion and embayment by the enclosing hematite cement (Fig. 11C, D). Some precursor tuffaceous materials are still seen embedded within the formed hematite cement (Fig. 11D).

Similar mechanism of the formation of the volcaniclastic red beds by the direct hematitization of the tuffaceous materials was postulated by Mesaed (2004b) in the volcaniclastic red beds underlying the Oligocene volcanic in north Abu Roash area, north Cairo, Egypt. Also, Taj et al. (2010) postulated the formation of the hematite of the volcaniclastic red beds of wadi Halwate area, Ablah district, Saudi Arabia, either by the direct hematitization of the tuffaceous materials specially in the oxidized depositional environments dominated in the upper parts of the shallowing-upward cycles or by the hematitization of the formed green celadonitic clays of the middle parts of the depositional cycles.

3. 4. 4. 2. Hematitization of the volcanic grains

In the volcaniclastic red bed of the 3th, 4th, and 5th cycles, the volcanic grains are suffered from intensive hematitization and formation of black hematitic films and coating around these grains (Fig. 11E, F). Also, the mafic minerals of these volcanic rock fragments become completely hematitized giving rise to goethite and hematite.

3. 4. 4. 3. Hematitization of the green celadonitic clays

This type of hematitization represents the main processes in the formation of the volcaniclastic red beds of the study area. The presence of green celadonitic siltstone and sandstone beds in the middle parts of the shallowing-upward cycles overlain by the volcaniclastic red beds confirm the formation of these red beds by the diagenetic hematitization of the precursor red staffs by the oxygenated pore spaces water.

The hematization is of the green celadonitic in the basalt flows terminated the first cycle. These are represented by green celadonitic clay laths and shreds (Fig. 12A). These laths and shreds become progressively of yellow and blood red colors (Fig. 12B). Within the formed blood red Fe-oxyhydroxides, small irregular relicts of the precursor green laths are still preserved (Fig. 12C, D).

Ultimate stages of diagenetic recrystallization and dehydration of the blood red amorphous iron oxyhydroxides led to the formation of black hematite patches and domains (Fig. 12E).

The formation of the red beds and ironstones by the hematitization of the green clays have been postulated for the formation of the ferric oxides throughout the penecontemporaneous oxidation of green chamositic clays, prior to burial, (Dunhan, 1960; Hunter, 1970; Sheldon, 1970; Parron and Nahoon, 1980; Guerrak, 1987 & 1988; Chauvel and Guerrak, 1989; Dressen, 1989; Mesaed and Surour, 1998 and Mesaed, 2004a, b). Others preferred the formation of ferric oxides and hydroxides by late stage burial diagenesis of green chamositic clays (Cotter and Link, 1993).

3. 4. 4. 4. Hematitization of Fe- Mg mafic minerals of basalt and dolerite

This is evidenced by the presence of black iron minerals (mostly goethite and hematite) intersected and parallel to the cleavage planes of the precursor pyroxene crystals (Fig. 12F). Complete and ultimate stage of hematitization and disruption of the formed iron minerals led to the formation of black (hematite, goethite) crystals, longitudinal laths and irregular crystallites (Fig. 12G, H).

4. DISCUSSION AND DEPOSITIONAL MODEL

From the stratigraphic and sedimentologic points of views, it is concluded here that, the succession of Tayibit El Esm area, shows very clear criteria supporting its deposition during interplay between volcanic activities and sedimentation. This is evidenced by the predominance of the grey tuffaceous mudstones in the lowermost part of cycle 1 and the predominance of green celadonitic tuffaceous mudstones in the lower and middle parts of the 2nd and 3rd cycles. Toward the upper part of the succession, the 4th, 5th and 6th cycles become composed entirely from red hematitic siltstones and sandstones which reflects the deposition in shallower conditions than that predominated during the deposition of the 1st , 2nd , and 3rd cycles. The deposition of silicified stromatolitic carbonates in the topmost part of the succession reflects deposition during periods of volcanic cession and very low volcaniclastic input which led to the carbonate deposition.

From the field, meg- and microscopic description it is concluded here that, the volcaniclastic red beds of the study area are formed during the following stages:

1) Deposition of the basic to intermediate volcanic constituents in slightly deeper back arc depositional setting which show progressive upward shoaling contemporaneous with the volcanic activities (Fig. 13A).

2) Syn- and post depositional authigenesis of green celadonitic clays in dysaerobic environments as a result of Fe^{2+} , Mg activities and the presence of Si and Al from the degradation of the volcanic ash. Similar mechanism of authigenesis of green marine clays along the sediments/water interface has been previously postulated by Mesaed (1999a, b) and Mesaed and Surour (2000). The formed green celadonitic clays are of variable organic matter content and also of variable Fe^{2+} content as a result of the vertical and lateral variation in the predominated micro physic-chemical conditions (Mesaed, 2004). This variation control in the degree of oxidation (hematitization) of these green celadonitic clays during the diagenetic processes (Fig. 13B).

3) The diagenetic hematitization of the green celadonitic clays as well as the unceladonitized tuffaceous materials of the middle and upper parts of the depositional cycles and the formation of goethite, hematite and iron-oxyhydroxides (Fig. 13C). The is dominated during the progressive shoaling where the depositional environment becomes shallow and of low organic matter content and of high ferric iron activities, this will led to the deposition of oxidized celadonitic clays of high ferric iron content and of low organic matter content which facilitate its oxidation into iron oxides and iron oxyhydroxides. Similar mechanism of variation in the degree of hematitization of the green clays as a result of the original variation in the micro-physico-chemical conditions was described by Mesaed (2004a) in the glauconitic ironstones of Gabal Qalamoon area, western Desert, Egypt, and

4) The deposition of the carbonates in the uppermost parts of the volcaniclastic succession during restricted time periods of very low volcaniclastic input dominated during cession of volcanic activities.

5) The studied volcaniclastic green and red beds-bearing succession of Tayibit El Esm must be followed laterally and vertically within the overall volcano-sedimentary succession of Ablah district. It represent a distinctive short-live time period of rifting and subaqueous volcanism.

5. REFERENCES

Allcott, G. H., 1969. Diamond Drilling at Ablah Ancient Mine: Annual Report of the Directorate General for Mineral Resources. Saudi Arabia, (September 1968 to September 1969), 32-43.

Brown, G.F., and Jackson, R.O., 1960. The Arabian shield: International geological Congress, XXI Session, Norden, Part IX Precambrian stratigraphy and correlations, 69-77.

Bryan, S.E., Fielding, C.R., Holcombe, R.J., Cook, A., Moffitt, C.A., 2003. Stratigraphy, facies architecture and tectonic implications of the Upper Devonian to Lower Carboniferous

Campwyn Volcanics of the Northern New England Fold Belt. Australian Journal of Earth Sciences. 50, 377–401.

Bull, S.W., Cas, R.A.F., 1991. Depositional controls and characteristics of subaqueous bedded volcaniclastics of the Coger Devonian Snowy River Volcanics. Sedimentary Geology 74, 189–215.

Bull, S.W., Cas, R.A.F., 2000. Distinguishing base-surge deposits and volcaniclastic fluviatile sediments: an ancient example from the Lower Devonian Snowy River Volcanics, south-eastern Australia. Sedimentology 47, 87–98.

Cas, R.A.F., Busby Spera, C., 1991. Volcaniclastic Sedimentation. Sedimentary Geolgy 74. 362 pp.

Chauvel, J. J. and Guerrak, S.,1989. Oolitization processes in Paleozoic ironstones of France, Algeria and Libya. In: Young, T.P. and Taylor W. E. G. (eds.) Phanerozoic ironstones. Geol. Soc. London, Special Publication 46, 165-174.

Cotter, E. and Link,J, E., 1993. Deposition and diagenesis of Clinton ironstones (Silurian) in the Appalachian Foreland Basin of Pennsylvania. Bulletin of the Geologic Society of America 105, 911-922.

Dreesen, R., 1989. Oolitic ironstones as event-stratigraphical marker beds within the upper Devonian of the Aedenno -Rhenish Massif. In: Young, T.P. and Taylor, W.E.G. (eds) Phanerozoic ironstones. Geologic Society of London, Special Publication 46,65-78.

Dunhum, K. C., 1960. Syngenetic and diagenetic mineralization in Yorkshire. Proceeding of the Yorkshire geologic Scoiety 232, 229-284.

Goldsmith, R., 1966. Mineral resources of the southern Hijaz quadrangle, Kingdom of Saudi Arabia: U.S. Geol. Survey Saudi Arabia Project, Tech. Ltr. 78, 6-17, 51, and 72-74.

Guerrak, S., 1987. Metallogenesis of cratonic oolitic ironstone deposits in the Beld el mass, Azzel matti, Ahnet and Moudir basins, Central Sahara, Algeria. Geologic Runudsch 76, No. 3, 903-922.

Guerrak, S., 1988. Paleozoic marine sedimentation and associated oolitic iron-rich deposits, Tassilis N Aijer and Illizin basin, Saharan Platform, Algeria, Eclogae Geologicae Helvetiae 81, 457-485.

Hunter, R. E., 1970. Iron sedimentation in the Clinton group of the central applachian basin. Unpublished Ph.D thesis, Johns Hopkins University, Maryland, 416P.

Johnson, P.R., 2006. Explanatory notes to the map of Proterozoic geology of western saudi Arabia, technical report SGS-Tr-2006-4.

Kuenzi, W.D., Horts, O.H., McGehee, 1979. Effect of volcanic activity on fluvio deltaic sedimentation in a modern arc-trench gap, southwestern Guatemala. Geologic Society America Bulletin, 90, 827–838.

Martí, J., 1996. Genesis of cristal-rich volcaniclastic facies in the permian red beds of the Central pyrenees (NE Spain). Sedimentary Geology 106, 1–19.

Mesaed, A. A., 1999a. Stratigraphic setting and paleoenvironments of the Bartonian- Priabonian glaucony facies of the northern part of the Western Desert, Egypt. Egyptian Journal of Geology 43/2, 1-27.

Mesaed, A. A., 2004a. Mechanism of Formation of the Upper Eocene Glauconitic Ironstones and Red Beds of Gabal Qalamoon area, Western Desert, Egypt. Egyptian Journal of Geology 48, 17-44.

Mesaed, A. A., 2004b. Mechanism of formation of the Oligocene volcaniclastic red beds and the associated tephra deposits, north Abu Roash area, Egypt. Proceedings of the 7th Int. Conference, Geology of the Arab World, GAW 7, Cairo University, 165-182.

Mesaed, A. A. and Surour, A. A., 2000. Mineral chemistry and mechanism of formation of the Bartonian glaucony of El Gedida Mine, El Bahariya Oases, Egypt. Egyptian Mineralogist 12, 1-28.

Mesaed, A. A. Surour, A. A., 1998. Mineralogy and geochemistry of the Bartonian stratabound diagenetic and lateritic glauconitic ironstones of El Gedida mine, El Bahariya Oases, Egypt. Proceedings of the 4th International Conference, Geology of the Arab World 1, 509-540.

Mesaed, A.A., 1999b. Origin and fabric evolution of the glaucony facies of the northern part of the Western Desert, Egypt. Egyptian Journal of Geology 43/2, 29-54.

Meyer, D.F., Dodge, J.E., 1988. Post-eruption changes in channel geometry of streams in the Toutle River drainage basin, 1983–1985, Mount St. Helens, Washington. Open- File Report. 87-549. U.S. Geological Survey. 226 pp.

Nakayama, K., Yoshikawa, S., 1997. Depositional processes of primary to reworked volcaniclastic on an alluvial plain: an example from the Lower Pliocene Ohta tepha bed of the Tokai Group, central Japan. Sedimentary Geology 107, 211–229.

O'Halloran, G.J., Gaul, A.J., 1997. Sedimentary responses to sub-aerial felsic volcanism from the Late Devonian–Early Carboniferous northern Macalister Synclinorium, southeastern Australia. Sedimentary Geology 109, 209–232.

Paredes, J.M., Foix, N., Colombo Piñol, F., Nillni, A., Allard, J.O., Marquillas, R.A., 2007. Volcanic and climatic controls on fluvial style in a high-energy system: the Lower Cretaceous Matasiete Formation, Golfo San Jorge Basin, Argentina. Sedimentary Geology 202, 96–123.

Parron, C. and Nahon, D., 1980. Red bed genesis by lateritic weathering of glauconitic sediments., Journal of the Geological Society of London 137, 689 - 693.

Riggs, N., Busby-Spera, C.J., 1990. Evolution of a multi-vent volcanic complex within a subsiding arc graben depression: Mount Wrightson Formation, Arizona. Geologic Society American Bulletin 102, 1114–1135.

Riggs, N.R., Hurlbert, J.C., Schroeder, T.J., Ward, S.A., 1997. The interaction of volcanism and sedimentation in the proximal areas of a mid-Tertiary Volcanic Dome Field, Central Arizona, U.S.A. Journal Sedimentary Research 67 (1), 142–153.

Segschneider, B., Landis, C.A., Manville, V., White, J.D.L., Wilson, C.J.N., 2002. Environmental response to a large, explosive rhyolite eruption: sedimentology of post-1.8 ka pumice-rich Taupo volcaniclastics in the Hawke's Bay region, NewZealand. Sedimentary Geology 150, 275–299.

Sheldon, R. P., 1970. Sedimentation of iron-rich rocks of Llandovery age (Lower Silurian) in the southern Appalachian basin, in Berry, W. B. N. and Boucot, A. J. (eds.), Correlation of the northern American Silurian Rocks: Geologic Society of America special paper 102, 107-112.

Smith, G.A., 1987. The influence of explosive volcanism on fluvial sedimentation: the Deschutes Formation (Neogene) in central Oregon. Journal of Sedimentary Petrology 57, 613–629.

Smith, G.A., 1991. Facies sequences and geometries in continental volcaniclastic sediments. In: Fisher, R.V., Smith, G.A. (Eds.), Sedimentation in Volcanic Settings. SEPM, Special Publication 45, pp. 109–121.

Smith, R.C.M., 1991. Landscape response to a major ignimbrite eruption, Taupo Volcanic Center, New Zealand. In: Fisher, R.V., Smith, G.A. (Eds.), Sedimentation in Volcanic Settings. SEPM, Special Publication 45, pp. 123–137.

Taj, R. J.; Mesaed, A. A.; Moufti, A.; Qari, M. A.T. and Matsah, M. I., 2010. Origin and Diagenetic History of the fluvio-lacustrine/ deltaic volcaniclastic red beds, W. Girshah-W. Halwate, Ablah District, Western Arabian Shield, Saudi Arabia. Fifth International Conference on the Geology of the Tethys Realm, South Valley University 227-248.

Theobald, P. K. ,Jr and Thompson, C. E., 1966. Geology and geochemistry of a part of the Ablah Formation Rumur, Kingdom of Saudi Arabia: U.S. Geol. Survey Saudi Arabian Project Tech. Ltr. 88.

Trent, V. A., 1966. Mineral investigations in the Agig area, Saudi Arabia: U.S. Geol. Survey Saudi Arabian Project Tech.Ltr. 38.

Trent, V. A. and Sultan, G. H., 1966. a geological and mineral reconnaissance of the Ablah Formation and the Kamdan Anomaly, South Agig area, Saudi Arabia: U.S. Geol. Survey Saudi Arabian Project Tech. Ltr. 68.

Umazano, A.M., Bellosi, E.S., Visconti, G., Melchor, R.N., 2008. Mechanisms of aggradation in fluvial systems influenced by explosive volcanism: an example from the Upper Cretaceous Bajo Barreal Formation, San Jorge Basin, Argentina. Sedimentary Geolgy 203, 213–228.

Van Houten, F. B., (1972. Iron and clay in tropical Savanna alluvium, Northern Colombia: A Contribution to the origin of red beds. Geologic Society American Bulletin 83, 2761-2772.

Van Houten,F. B., 1968. Iron oxides in red beds. Bulletin of the Geologic Society of America 79, 399-416.

Vessel, R.K., Davies, D.K., 1981. Non-marine sedimentation in an active fore-arc basin. In: Ethidge, F.G., Flores, R.M. (Eds.), Recent and Ancient Non-marine DepositionalEnvironments. Spec. Publ. Soc. Econ. Paleontol. Mineral 31, pp. 31–45.

Waresback, D.B., Turbeville, B.N., 1990. Evolution of a Plio-Pleistocene volcanogenic alluvial fan: the Puye Formation, Jemez Mountains, New Mexico. Bulletin of the Geologic Society of America.

Young, T.P., 1989. Phanerozoic ironstones: an introduction and review. In: Young TP, Taylor WEG (eds) Phanerozoic ironstones. Special Publication Geologic Society London 46, pp ix–xxv.

Zakir, F. 1972, Geology of the Ablah area, southern Hijaz Quadrangle, Kingdom of Saudi Arabia. M. Sc Thesis, South Dakota School of Mines and Technology, Rapid City, South Dakota, 66p.

Fig. (1): Geologic map of wadi Girshah- Gabal Ablah area (Taj e
Click here to download high resolution image

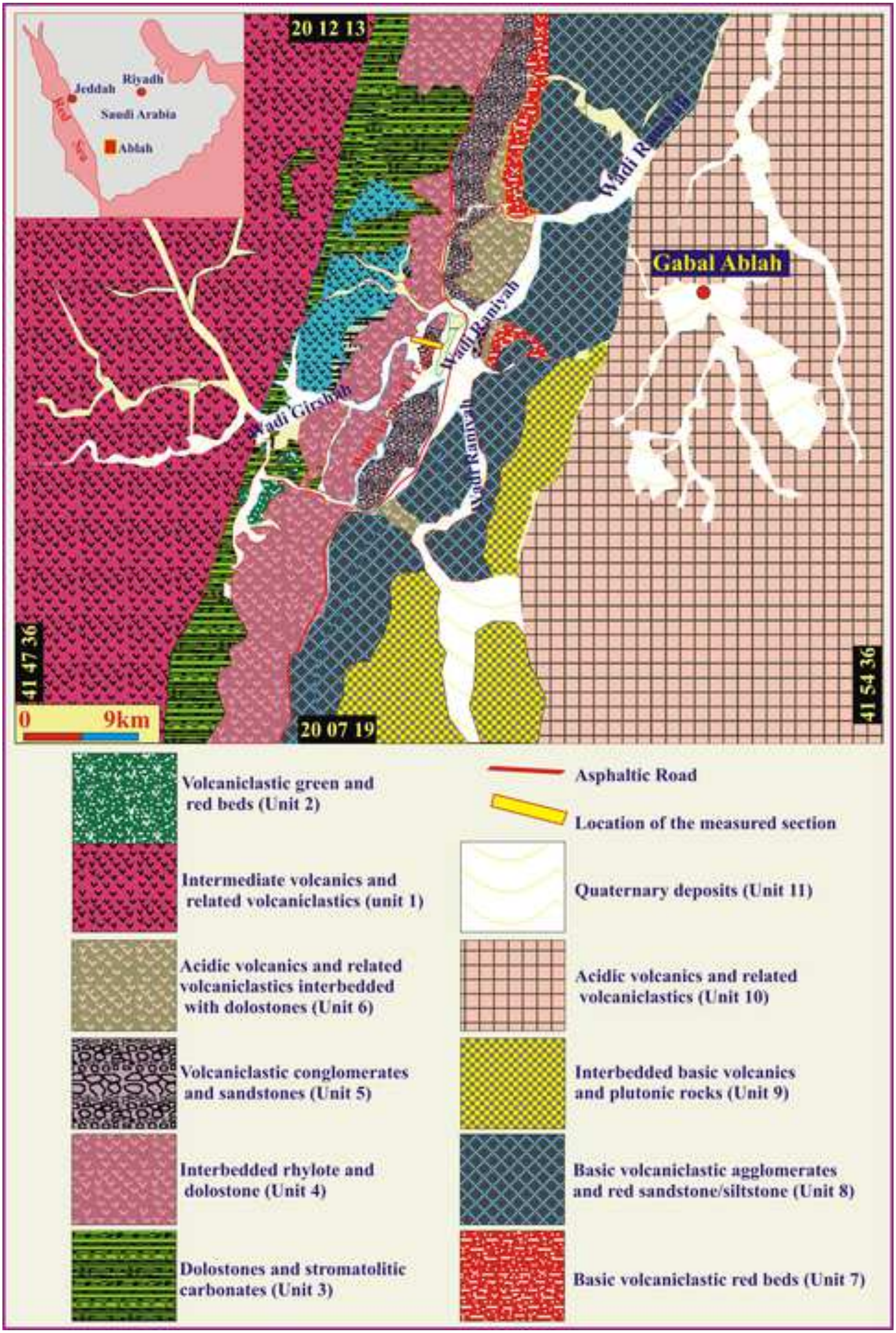

Fig. (2): A= Satellite image of wadi Giorshah- Tayibit El Esm ar

Click here to download high resolution image

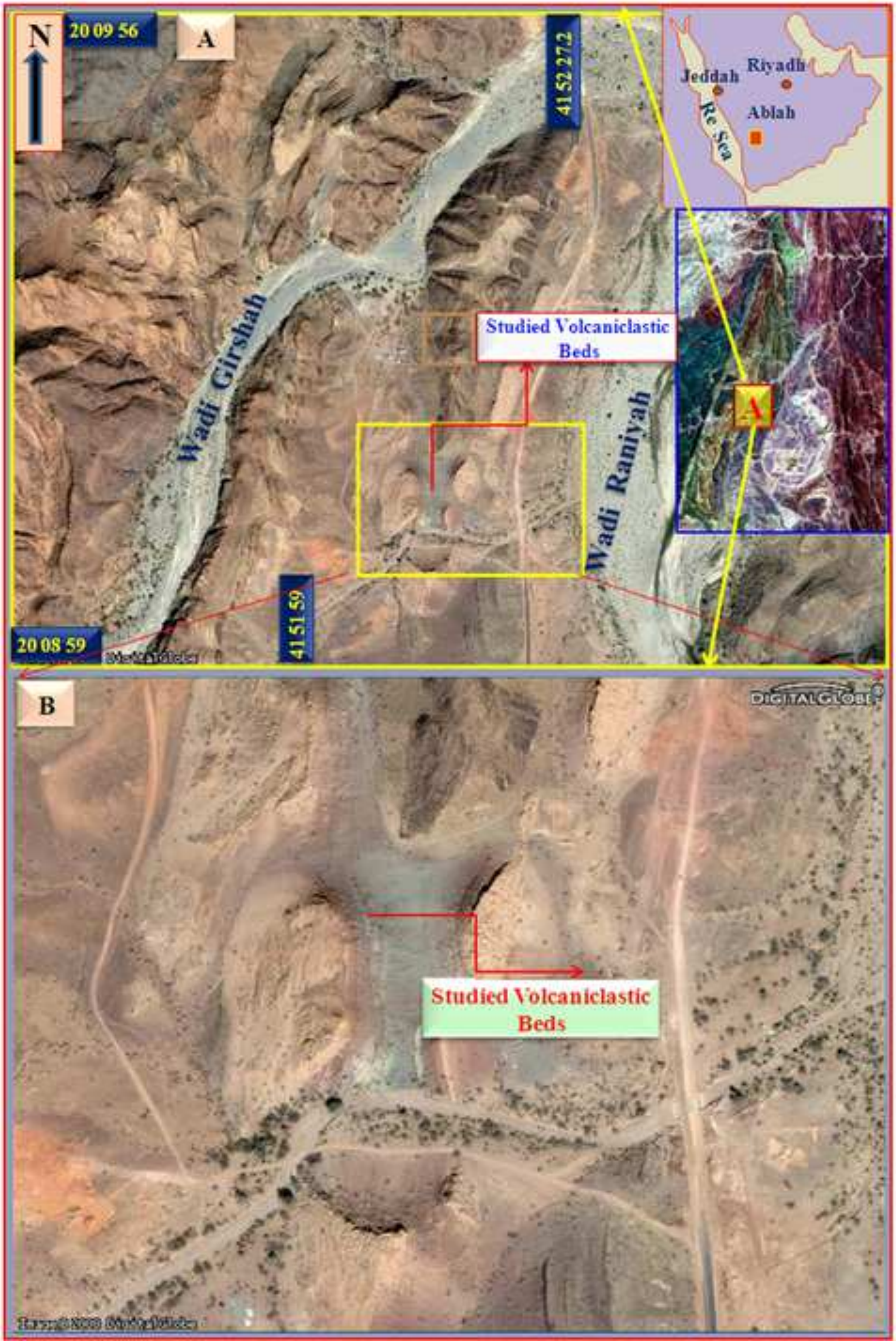

Fig. (3): A= Panoramic view showing the two limbs (eastern and w
Click here to download high resolution image

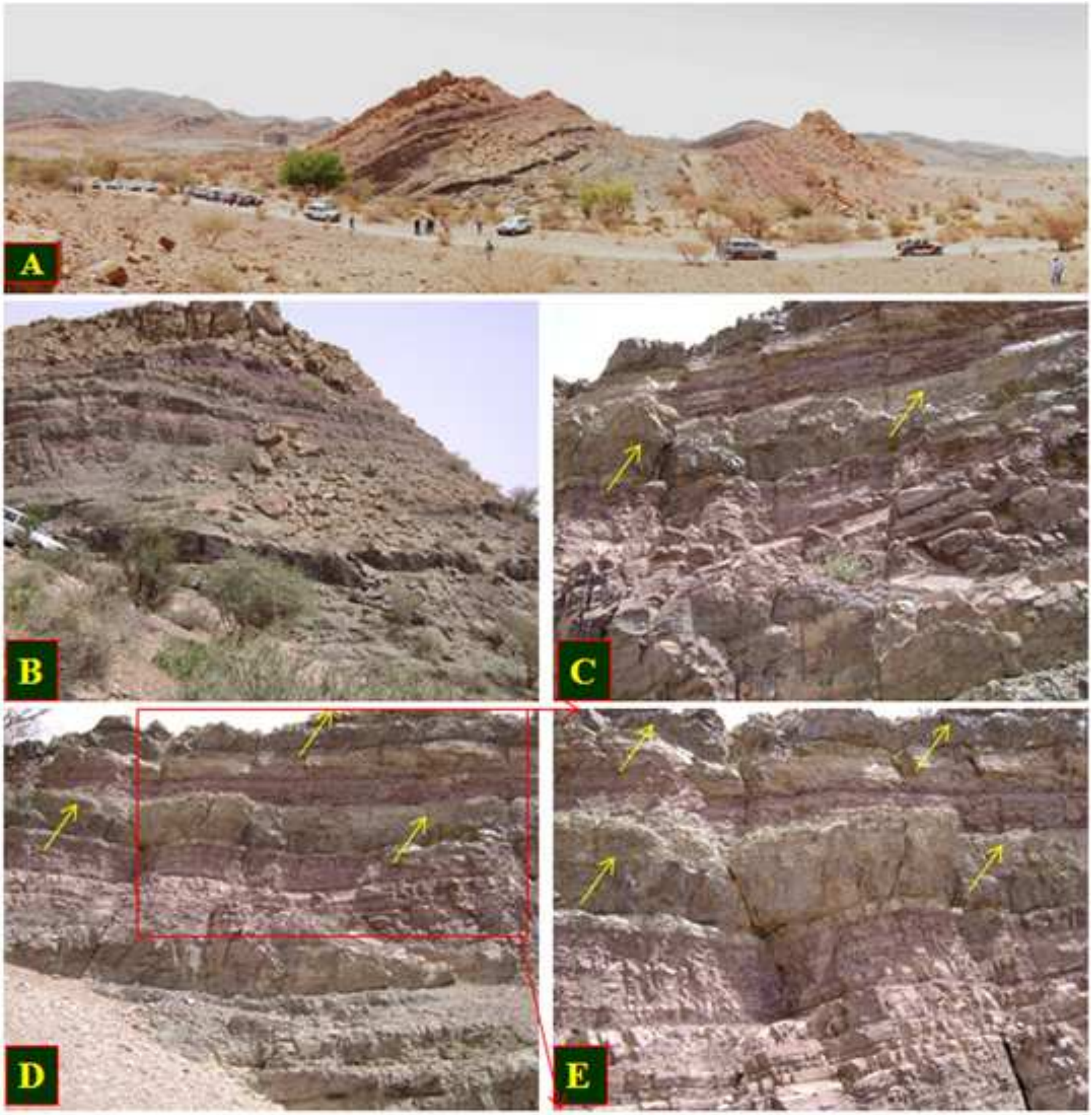

Fig. (4): Detailed stratigraphic section showing the shallowing-

Click here to download high resolution image

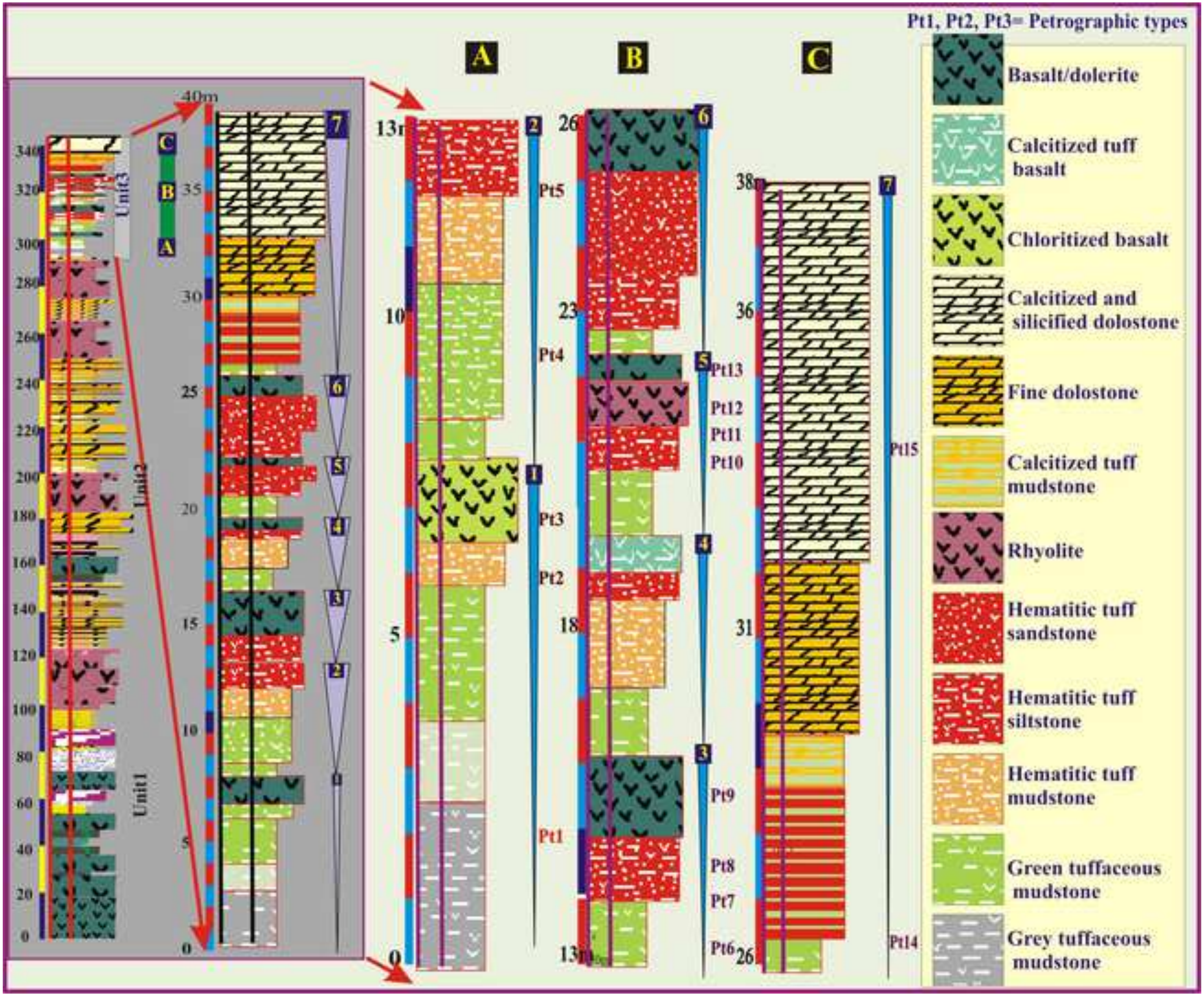

Fig. (5): A= Grey tuffaceous mudstone Pt1 which consists of bla
Click here to download high resolution image

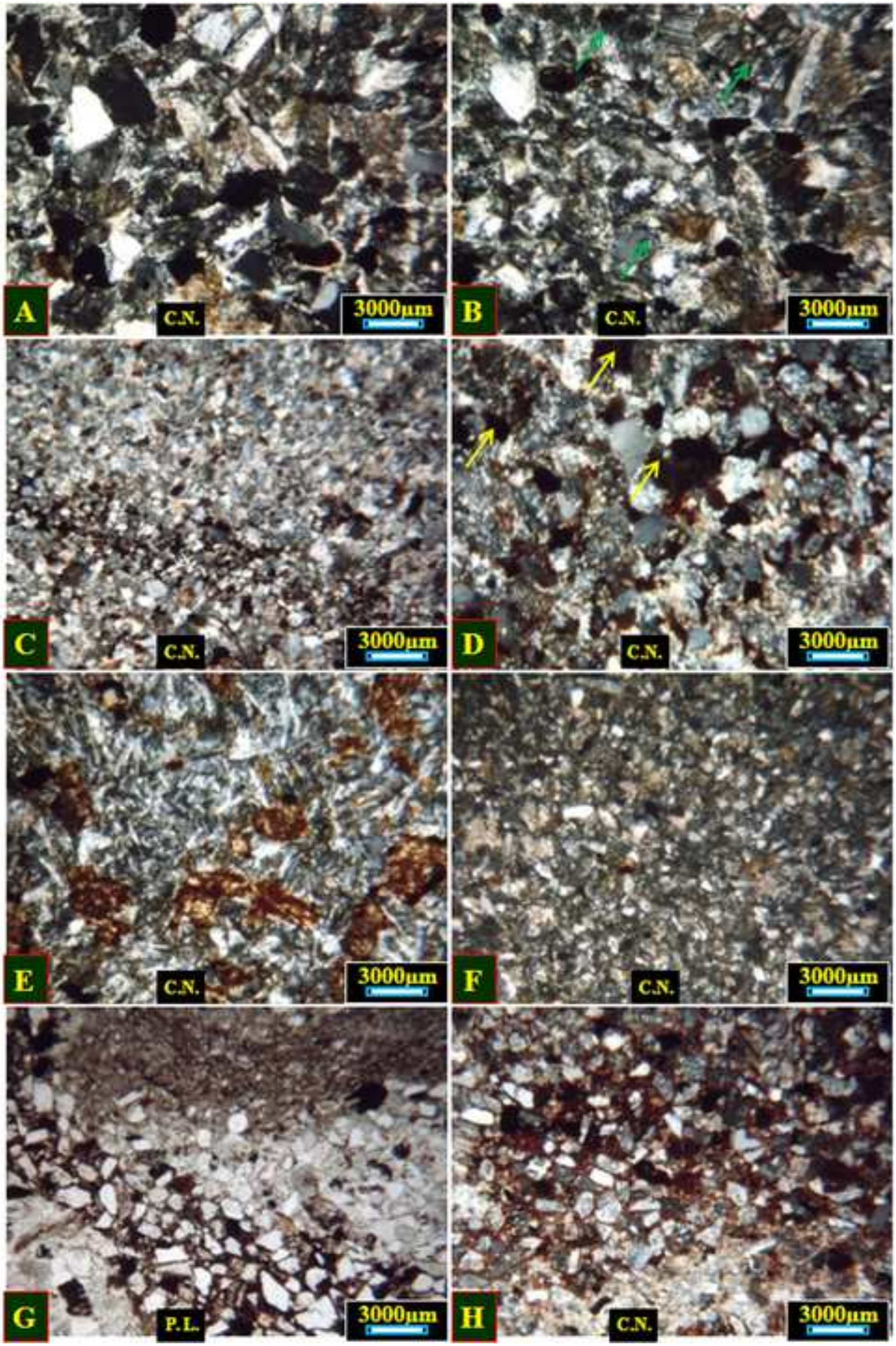

Fig. (6): A= The calcitized tuffaceous mudstone Pt6 which consis
Click here to download high resolution image

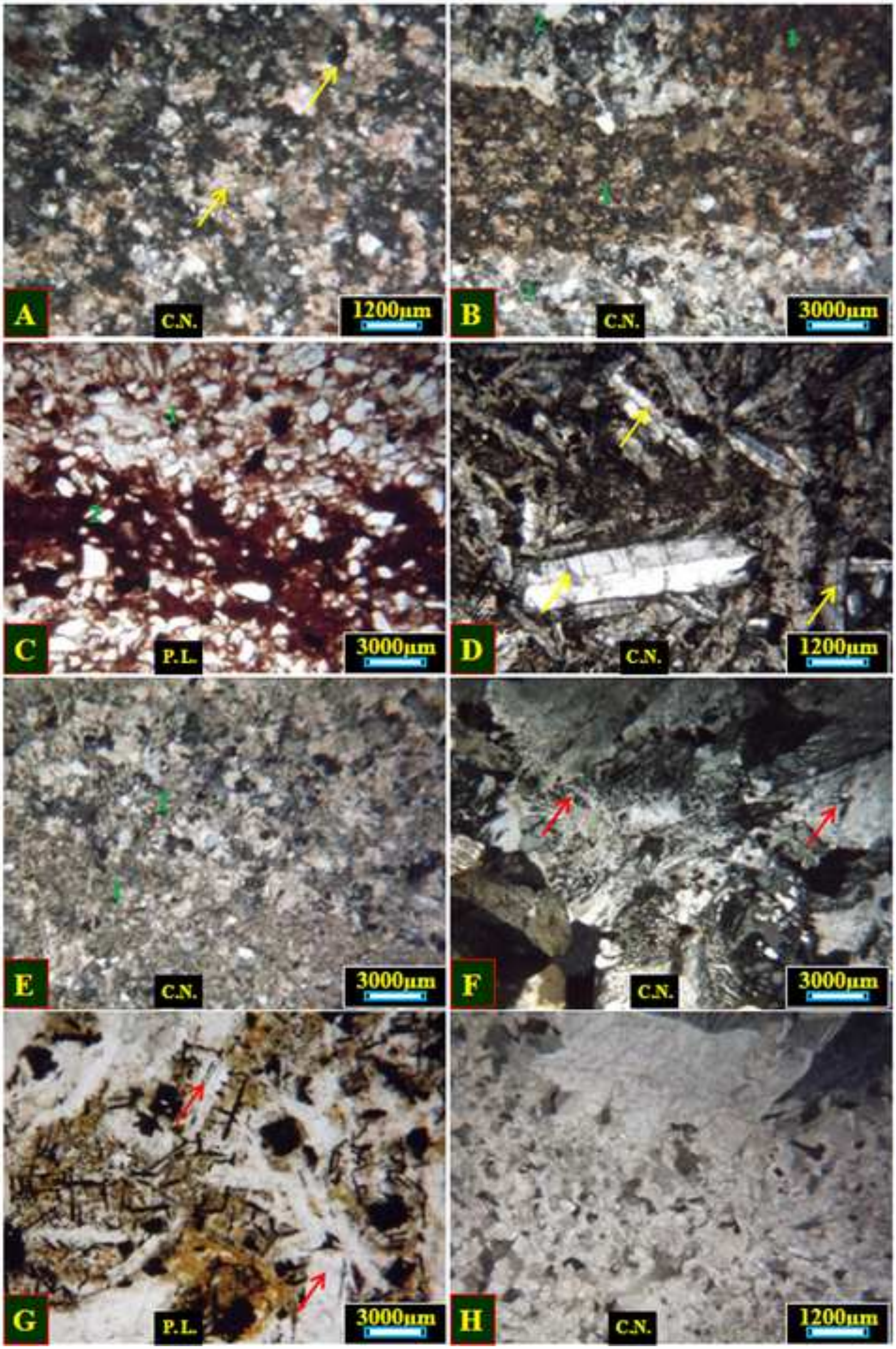

Table 1: Bulk XRF analyses of the different horizons of the gree
Click here to download high resolution image

Elements	21 Pt 1	22 Pt 2	23 Pt 3	24 Pt 4	25 Pt 5	26 Pt 6, 7	27 Pt 8	28 Pt 9	29 Pt 10	30 Pt 11	31 Pt 12	32 pt 13
TiO_2%	0.69	0.53	0.42	0.61	0.5	0.59	0.59	0.51	2.41	0.51	0.5	2.62
Al_2O_3%	28.43	26.18	6.19	14	11.83	11.86	15.14	13.28	17.66	11.83	11.1	18.56
Fe_2O_3%	5.22	4.27	5.17	3.49	4.2	4.5	4.36	4.47	9.25	3.87	3.14	10.01
CaO%	1.8	4.81	2.92	1.74	0.79	8.21	3.96	5.08	5.34	10.64	9.73	5.23
MgO%	3.14	4.26	0.48	3.3	6.91	6.35	6.06	5.69	5.35	7.74	9.5	4.03
MnO%	0.03	0.05	0.11	0.02	0.22	0.14	0.06	0.1	0.12	0.15	0.18	0.11
Na_2O%	2.13	1.95	2.35	1.74	0.69	1.63	2.18	1.97	2.18	1.5	1.94	2.14
K_2O%	2.02	1.6	0.13	1.72	1.74	0.57	1.36	1.61	0.79	0.74	1.18	1.81
Ag	0	0	1.6	0	0	0	0	0	0	0	0	0
As	0	0	0	0	0	0	0	0	0	0	0	0
Au	0	0	0	0	0	0	0	0	0	0	0	0
B	1699	2272	1195	1763	2476	2636	2612	2564	2506	2788	2712	2944
Ba	1238	1190	289	2766	376	984	1249	672	465	479	441	2184
Be	0	0	0	0	0	0	0	0	0	0	0	0
Bi	0	0	0	0	0	0	0	0	0	0	0	0
Cd	1	1	0.8	1.1	0.8	1	1	1	0.8	0.8	0.8	1.2
Co	15.6	12.2	5	11.4	12.2	15.6	13.4	13.8	63	15	13.8	67
Cr	367	112	8.2	216	87	44	101	99	60	77	150	54
Cu	18	20	23	13.6	5.8	70	5.4	3.2	35	70	34	58
Li	37	49	10	48	3	70	62	48	61	69	43	43
Mo	3.6	2.2	4.4	2.2	2.2	2	1.6	2.2	2.8	1.8	2.4	2.4
Ni	29	25	2	2	21	29	25	27	63	25	28	70
Pb	8.2	9.8	10.2	9.6	10.6	10.8	15.2	11.6	8.2	9.6	9.2	12.8
Sb	9.6	10	5.6	7.2	8	7.4	21	9.4	8.8	8.4	8.6	8.8
Se	3.8	3	6.8	12.8	3.8	8.6	6.4	6.4	3.2	6.2	3.4	7.8
Sr	131	168	40	241	129	206	148	133	496	160	146	382
Tl	0	0	2.2	0	0	5	0	0.6	6.6	0	0	4.8
V	96	80	16.2	72	59	70	82	71	215	55	69	235
Zn	56	67	117.4	61	66	92	75	65	100	85	58	107

Fig. (7): Geochemical relations between the different elements

Click here to download high resolution image

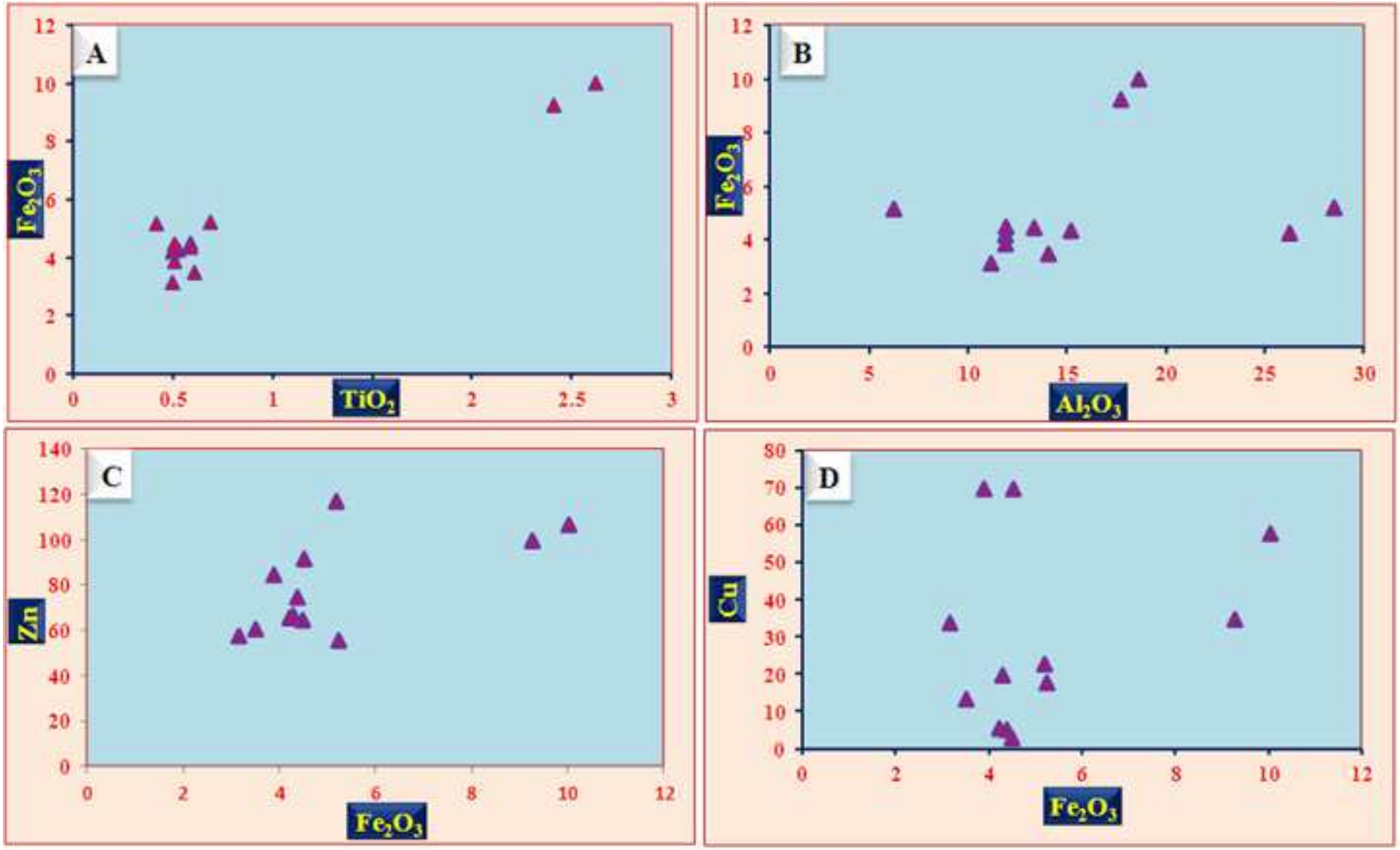

Fig. (8):: A, B= Initial stages of devitrification of tuffaceous
Click here to download high resolution image

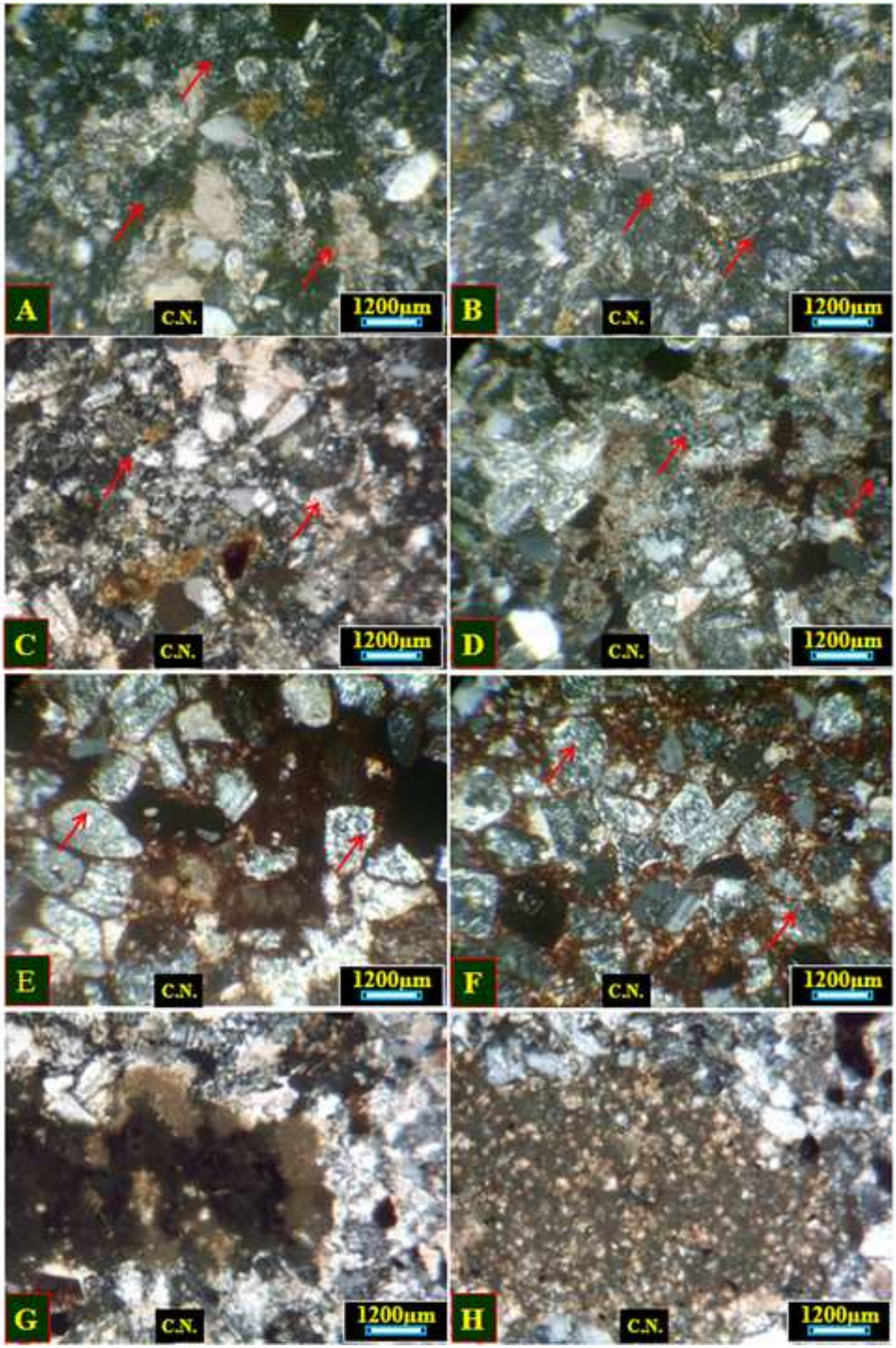

Fig. (9): A= The calcitization of tuffaceous materials and forma
Click here to download high resolution image

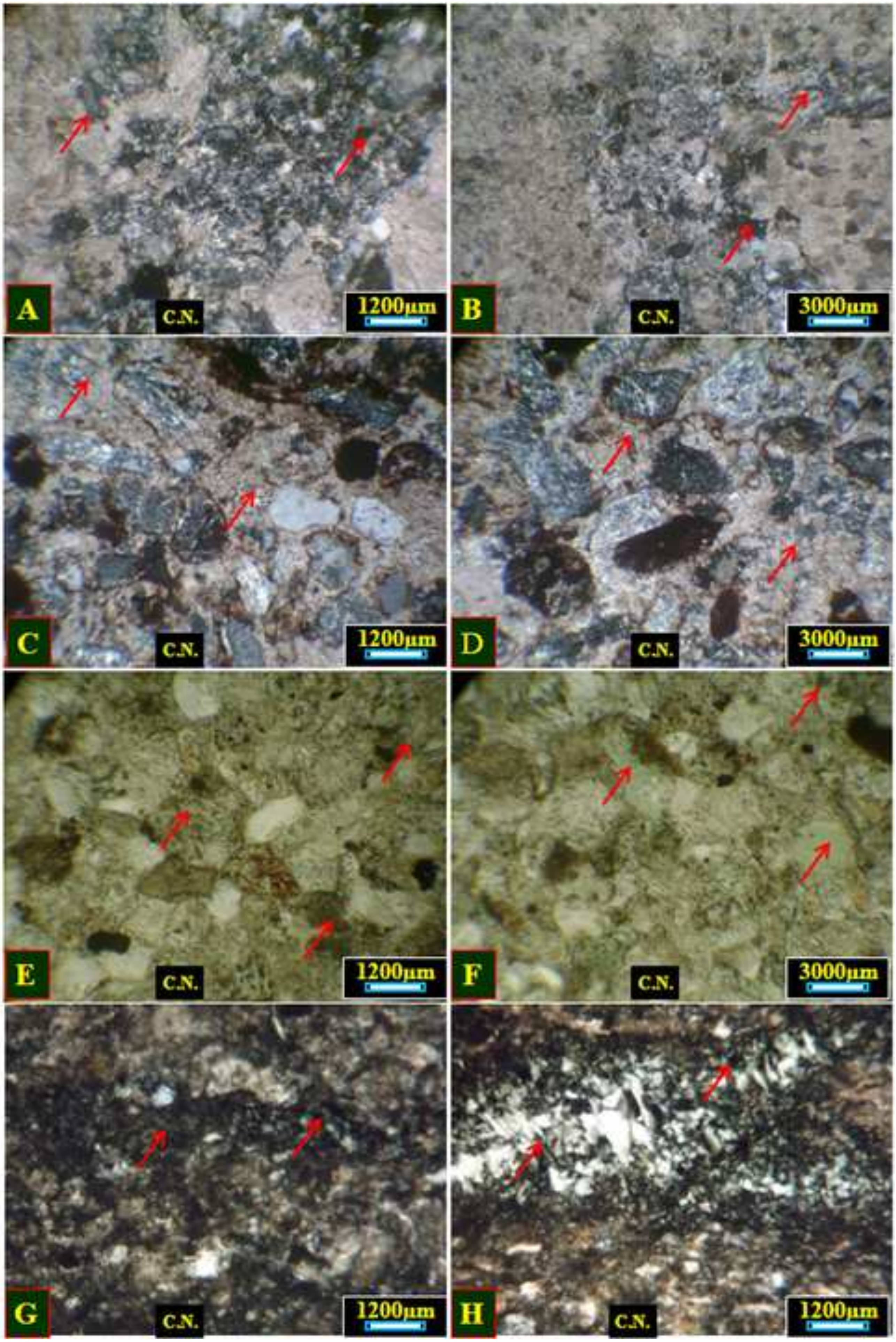

Fig. (10): A, B= Hematitization of different constituents of the
Click here to download high resolution image

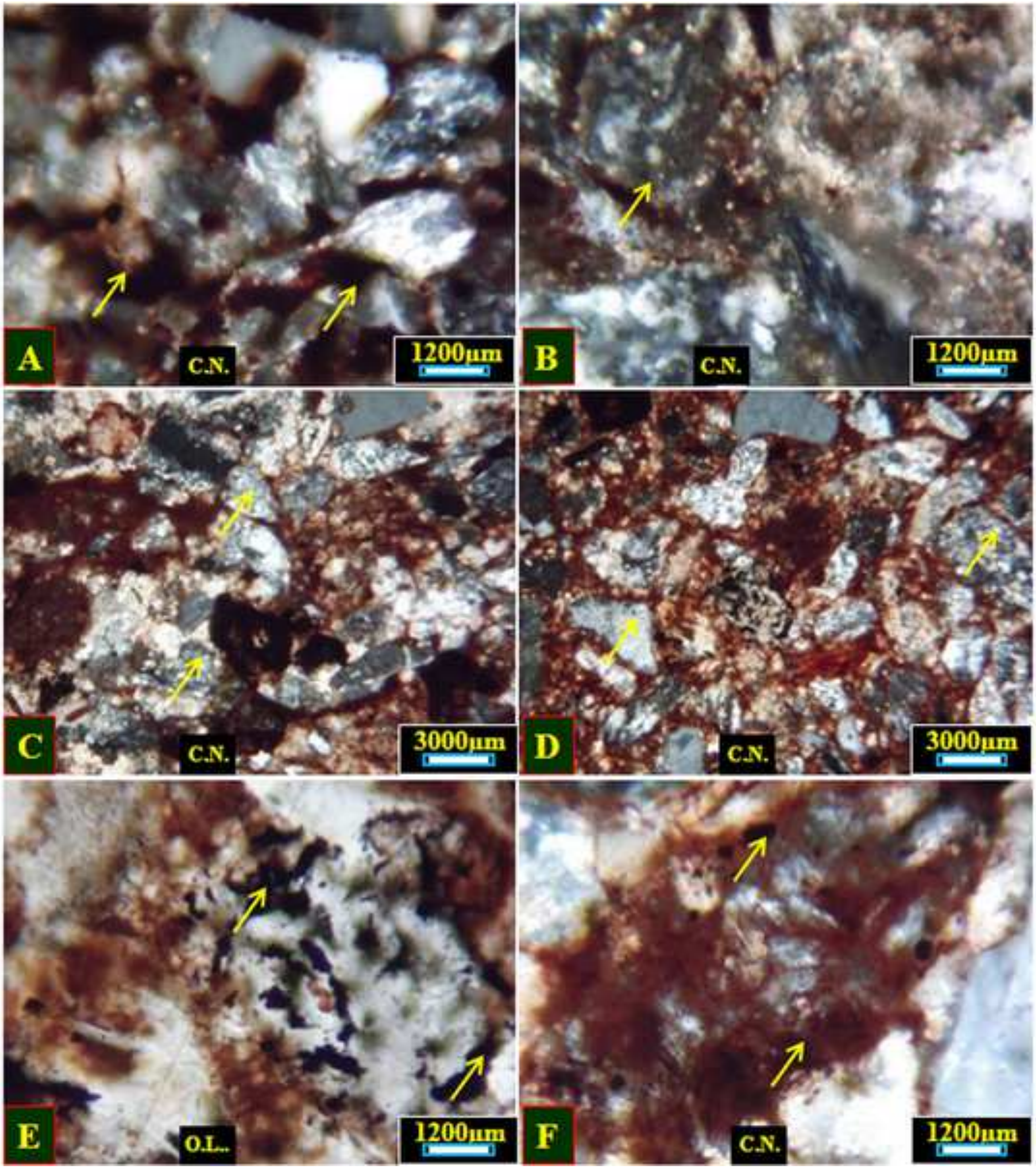

Fig. (11): A, B, C= The hematitization processes is evidenced by

Click here to download high resolution image

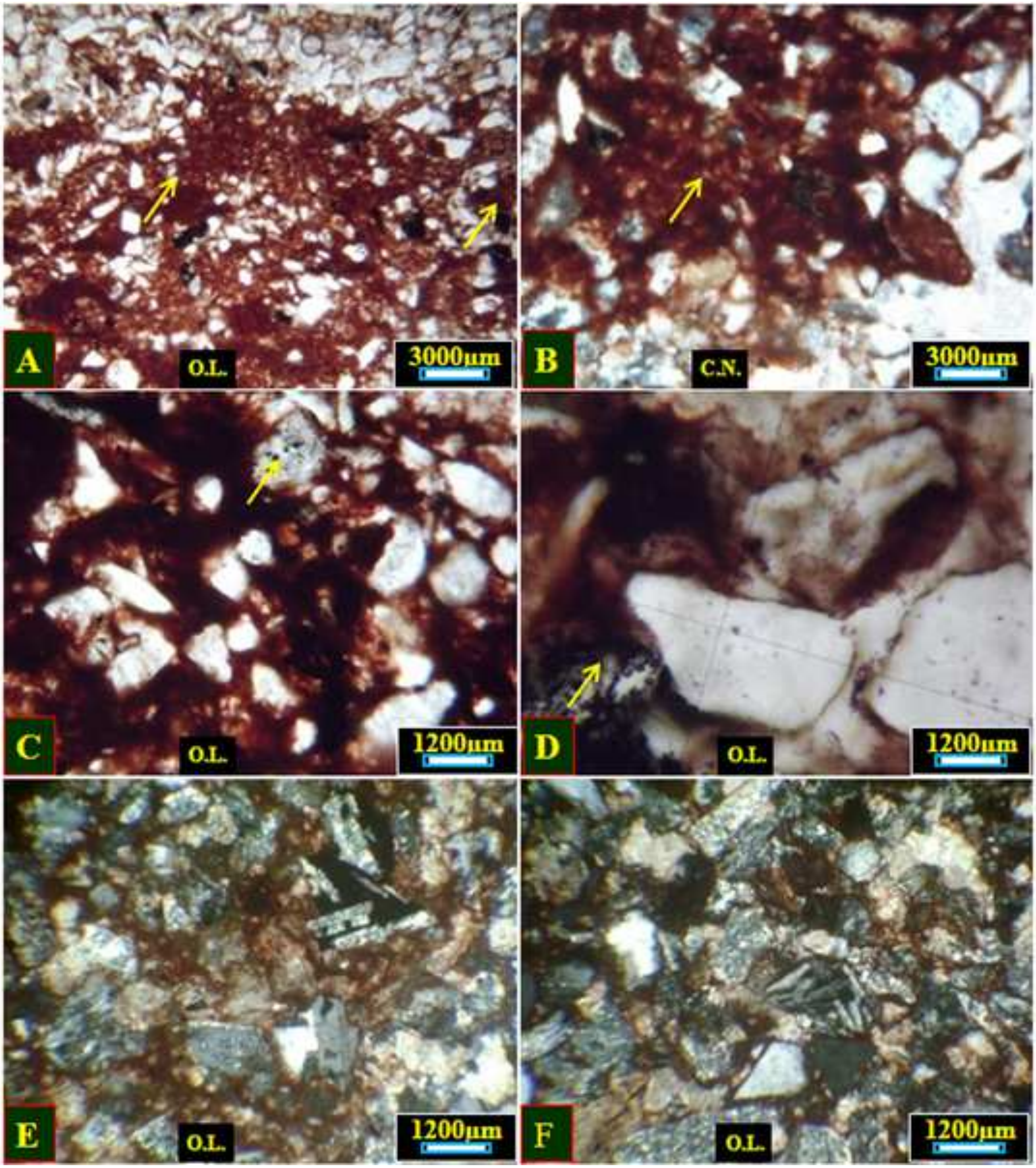

Fig. (12): A= The hematitization of the green green celadonitic
Click here to download high resolution image

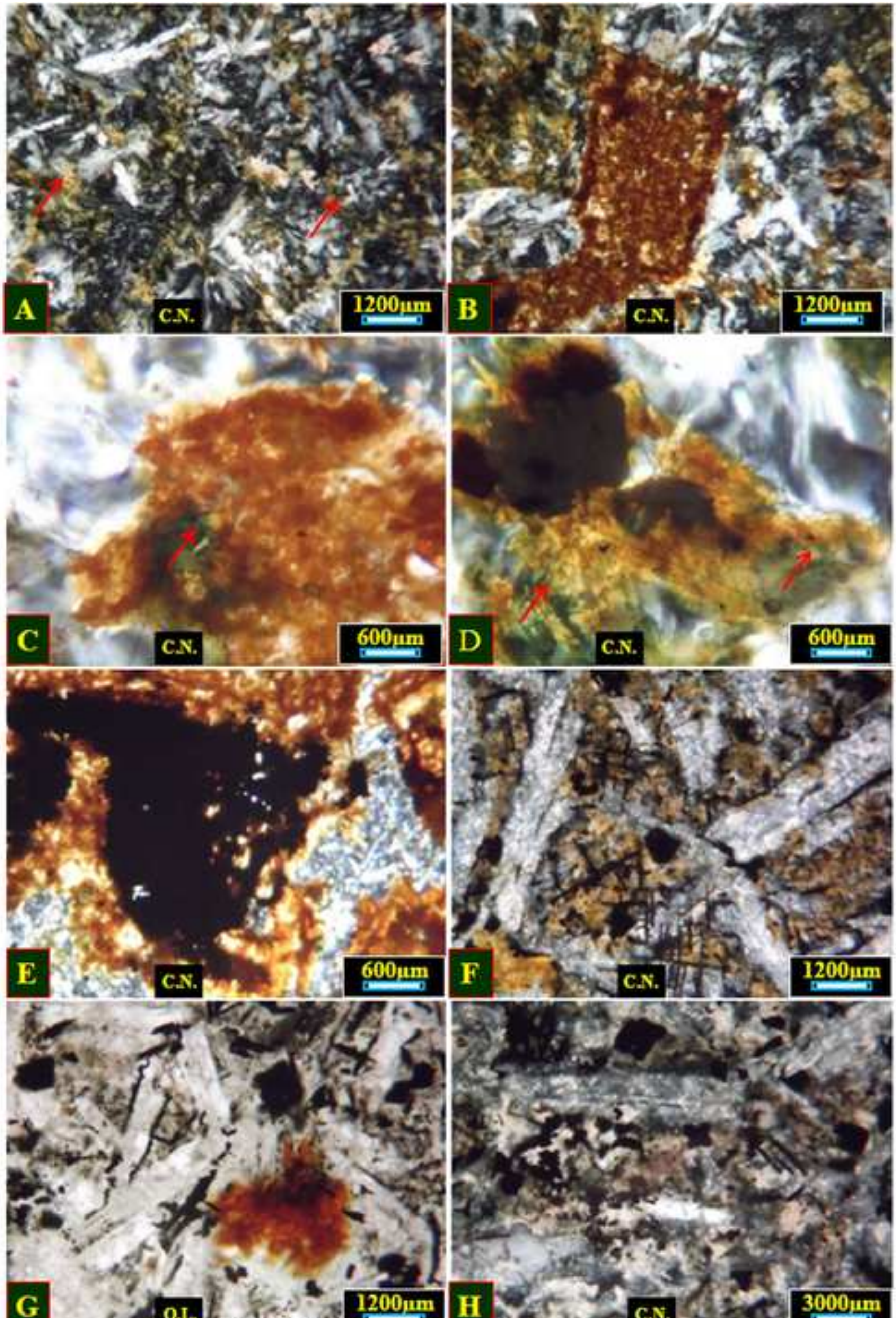

Fig. (13): A, B, C= The depositional and diagenetic evolution mo
Click here to download high resolution image

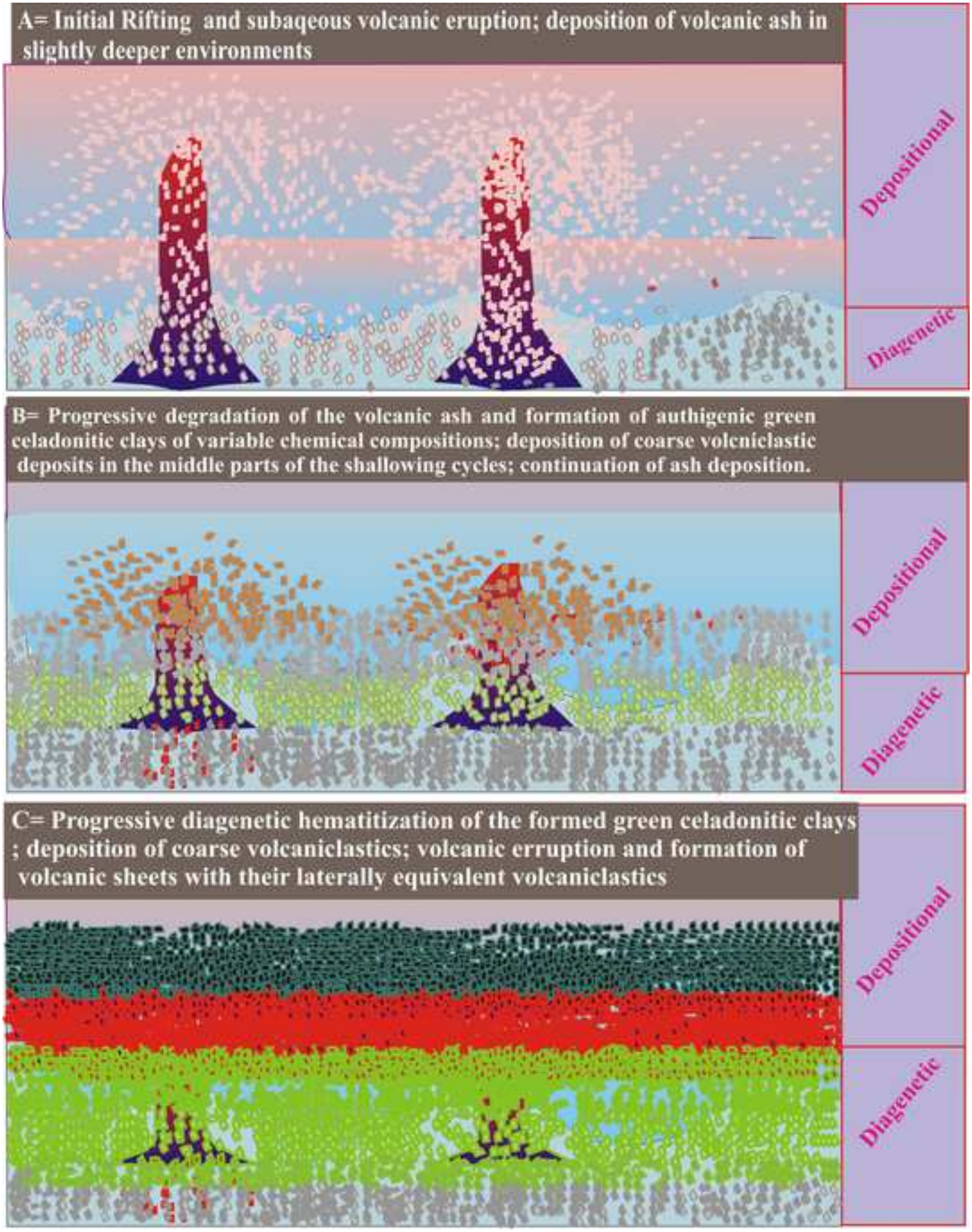

Figures Captions

Fig. (1): Geologic map of wadi Girshah- Gabal Ablah area (Taj et. al. 2010).

Fig. (2): A= Satellite image of wadi Giorshah- Tayibit El Esm area; **B**= Detailed satellite image of the double plunged anticline of Tayibit El Esm area showing the location of the studied volcaniclastic green and red beds.

Fig. (3): A= Panoramic view showing the two limbs (eastern and western) of the north-south double plunged anticline of Tayibit El Esm area; B= complete succession of the western limb of Tayibit El Esm double plunged anticline; C; D, D= The successive shallowing upward cycles which are terminated by black color basaltic flows (arrows).

Fig. (4): Detailed stratigraphic section showing the shallowing-upward cycles of Tayibit El Esm double plunged anticline.

Fig. (5): A= Grey tuffaceous mudstone Pt1 which consists of black isotropic tuffaceous material contains silt-sized quartz grains; B= Small authigenic feldspar crystals and numerous devitrified volcanic domains and patches (arrows); C= Hematitic tuffaceous siltstone Pt2 which consists of angular to subrounded silt-sized quartz grains (white) embedded in partially to completely hematitized interstitial tuffaceous matrix (black); D= Corrosion and and embayment of the quartz grains by the enclosing hematite cement forming dark patches and domains (arrows); E= The hematitized chloritized tuffaceous basalt Pt3 which consists of lath-like interlocked plagioclase crystals embedded in green intensively chloritized volcanic glass and olivine and pyroxene microlites (arrows); F= The green celadonitic tuffaceous mudstone / siltstone Pt4 which consists of green tuffaceous materials contain silt-sized quartz grains (white); G= The thinly laminated hematitic tuffaceous siltstone Pt5 which consists of rhythmically alternating Fe-rich clayey hematitic laminae (red) alternating with quartz-rich light laminae (light); H= Dark brown to black hematitic patches are present within blood red Fe-oxyhydroxides ground mass (reddish brown).

Fig. (6): A= The calcitized tuffaceous mudstone Pt6 which consists of green tuffaceous mud subjected to diagenetic calcitization and formation of micrite or microspar in between the quartz grains (arrows); B= The laminated calcareous siltstone pt7 which consists of laminated calcitized tuffaceous mudstone (1) and tuffaceous siltstone (2); C= The laminated tuffaceous hematitic sandstone Pt8 which consists of green celadonitic siltstone (1) parallel to reddish green slightly hematitic celadonitic siltstone (2); D= The hematitized trachytic doleritic basalt Pt9 which consists mainly of lath-like sanidine crystals (arrows) embedded in Ca- plagioclase crystals; E= The thinly laminated green celadonitic mudstone / siltstone Pt10 which consists of parallel laminated green celadonitic mudstone (1) and celadonitic siltstone (2); F= The myrmikitic fine Granite/Rhyolite Pt12 which consists of orthoclase, albite with less frequent quartz. It is characterized by the presence of myrmikitic texture (arrows); G= The celadonitized and chloritized doleritic basalt Pt13 which consists from highly disrupted intensively chloritized, celadonitized and finally oxidized olivine and pyroxene crystallites and ground mass in between calcitized Ca-plagioclase crystals (arrows); H= The green calcitized mudstone Pt14 which consists mainly of partially to completely calcitized tuffaceous mudstone.

Fig. (7): Geochemical relations between the different elements of the studied volcaniclastic red beds.

Fig. (8):: A, B= Initial stages of devitrification of tuffaceous materials and formation of non-crystalline and isotropic (arrows); C, D= Progressive stages of diagenetic recrystallization and formation of small quartz aggregates (arrows); E, F= Devitrification of the volcanic grains of the tuffaceous sandstones into microcrystalline quartz aggregates (arrows); G, H= The calcitization of the precursor tuffaceous materials of the peripheral parts of the black isotropic material (Fig. G) or by entire calcitization and formation of microcrystalline carbonate aggregates (Fig. H).

Fig. (9): A= The calcitization of tuffaceous materials and formation of microcrystalline calcite patches and domains (arrows); B= Ultimate stages of recrystallization led to the formation of blocky calcite showing some signs of silicification and formation of some quartz patches and domains (arrows); C, D= Entirely calcitization of the tuffaceous materials and formation of non crystalline micritic calcite in the interstitial spaces between the isotropic volcanic grains (arrows); E, F= The greening (celadonitization) of the precursor tuffaceous materials and the formation of the presence of green celadonitic clays in the interstitial spaces between volcaniclastic grains (arrows); G, H= Green celadonitic clay patches and domains within the precursor tuffaceous materials (arrows).

Fig. (10): A, B= Hematitization of different constituents of the volcaniclastics and formation of iron oxyhydroxides minerals (arrows); C, D= The devitrification of the volcanic grains and formation of aggregates of microcrystalline quartz (arrows); E, F= The diagenetic recrystallization and dehydration of the amorphous blood red phase (Geothite) in to the black massive hematite (arrows).

Fig. (11): A, B, C= The hematitization processes is evidenced by the patchy nature of the hematitic domains and the presence of slightly hematitized domains (arrows); D= Some precursor tuffaceous materials are still seen embedded within the formed hematite cement (arrows); E, F= The hematitization of the volcanic grains and formation of black hematitic films and coating around these grains (black).

Fig. (12): A= The hematitization of the green green celadonitic clay laths and shreds (arrows); B= The laths and shreds become progressively of yellow and blood red colors (arrows): C, D= Small irregular relicts of the precursor green laths are still preserved within the formed blood red Fe-oxyhydroxides, (arrows); E = Ultimate stages of diagenetic recrystallization and dehydration of the blood red amorphous iron oxyhydroxides led to the formation of black hematite patches and domains (black); F, G, H= The hematitization of Fe- Mg mafic minerals of basalt and dolerite and formation of black iron minerals (mostly goethite and hematite) intersected and parallel to the cleavage planes of the precursor pyroxene crystals.

Fig. (13): A, B, C= The depositional and diagenetic evolution model of the studied volcaniclastic red beds.

Tables Captions

Table 1: Bulk XRF analyses of the different horizons of the green and red volcaniclastic beds of Tayibit El Esm area.